JACS
JOURNAL OF THE AMERICAN CHEMICAL SOCIETY

ARTICLE

pubs.acs.org/JACS

Understanding the Molecular Mechanism of Enzyme Dynamics of Ribonuclease A through Protonation/Deprotonation of HIS48

Chang G. Ji[*,†,‡] and John Z. H. Zhang[*,†,‡,§]

[†]State Key Laboratory of Precision Spectroscopy, Department of Physics, East China Normal University, Shanghai 200062, China

[‡]Institute of Theoretical and Computational Science, Institutes for Advanced Interdisciplinary Research, East China Normal University, Shanghai 200062, China

[§]Department of Chemistry, New York University, New York, New York 10003, United States

Supporting Information

ABSTRACT: Molecular dynamics simulation is carried out to investigate the enzyme dynamics of RNase A with the HIS48 in three different states (HIP48 (protonated), HID48 (deprotonated), and H48A mutant). Insights derived from the current theoretical study, combined with the available experimental observations, enabled us to provide a microscopic picture for the efficient enzyme dynamics. Specifically, in the "closed" state or HIP48, the N-terminal hinge loop is intact and the enzyme remains in a relatively stable conformation which is preferred for catalytic reaction. Deprotonation of HIS48 induces the denaturing of this hinge-loop into a 3_{10}-helix, causing it to break the original interaction network around the loop-1 and drive the partial unfolding of the N-terminal. The enhanced dynamic motion of the N-terminal helix facilitates the release of the catalytic product (the rate limiting step) and speeds up the overall catalytic process. The current study established that HIS49 acts as a modulator for the transformation of conformational states through the perturbing of hydrogen bond networks across loop-1, the N-terminal helix, and other residues nearby. Our study suggests that HIS48 may also serve to transport loop-1's kinetic energy to the reaction center.

INTRODUCTION

RNase A (Ribonuclease A), an endonuclease that cleaves single-stranded RNA, is one of the most extensively studied enzymes in protein science.[1−3] It is a model system for studying protein folding, protein−ligand binding, thermodynamics and kinetics of enzyme reaction, and so forth. RNase A is a relatively small protein (124 residues) composed of six sheets and three helices with a deep cleft, formed by the N-terminal helix and C-terminal sheets, for binding RNA substrate (see Figure 1). RNase A has four disulfide bonds that help stabilize its native structure. The RNA substrate lies in the cleft and is cleaved by two catalytic histidines: His12 and His119.

RNase A is a monomeric enzyme that catalyzes the transphosphorylation of single-stranded RNA without the use of cofactors or metal ions. Although the chemistry involved in its catalytic process has been understood since the 1960s, it was also proposed that the enzyme's dynamical motions is also an important factor in determining RNase A's catalytic efficiency (see a recent review by Hammes[4]). Dynamical motions coupled to enzymatic reaction have been studied by experimental[5,6] and theoretical[7−10] researchers to investigate the contribution of protein dynamics to the catalytic power of RNase A. Early biochemical studies conducted by Hammes et al. using temperature jump techniques[5] determined that two conformational states exist in RNase A.[4,11] The equilibrium between these two states and the catalytic kinetics are pH-dependent,[12−17] and in particular, the residue HIS48 seems to play a special role in modulating the pH-dependent conformational transition.[18] This was verified from pH titration experiments of RNase A in which the discontinuity of HIS48's titration curve was observed.[19−23] NMR titration experiments confirmed that RNase A adopts different conformations in the crystal and in the solution.[24] It is also understood that the release of the product is the rate-determining step in the catalysis by RNase A.[6,25−29] More recently, advanced NMR relaxation and solvent isotope techniques have been employed to help unravel the mysterious relationship between the protein flexibility and catalytic power of RNase A.[29]

Since the information derived from the static crystal structure is limited and does not reflect conformational dynamics of protein in solution[24] due to crystal packing effects, molecular dynamics (MD) simulation of RNase A is carried out in the present work to help elucidate the dynamic role of His48 in relation to enzyme catalysis. Molecular dynamics simulation is an efficient tool for exploring correlated motions and

Received: July 5, 2011
Published: September 26, 2011

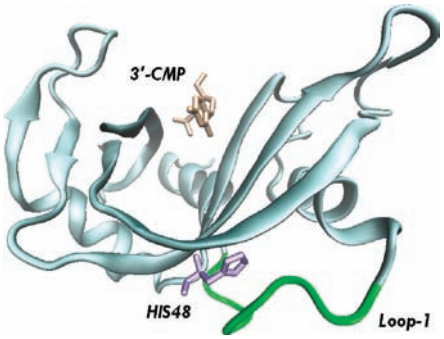

Figure 1. Structure of Rnase A bound with the catalytic product 3′-CMP. The 3′-CMP is highlighted in orange color, the HIS48 in violet, and the Loop-1 in green.

conformational changes of proteins. In the present study, different protonation states of HIS48, as well as the mutated state H48A, are studied in detail by MD simulation using AMBER99SB force field.[30] We hope that combining the computational result with the existing experimental observations will help delineate the dynamical mechanism that controls the catalytic efficiency of RNase A.

The present study aims to help understand dynamical origin of RNase A's catalysis in order to address specific experimental findings: (1) discontinuity of titration curve on HIS48 (which implies large conformational changes during the deprotonation process of HIS48[21]); (2) control of conformational change by the protonation state of HIS48 (observed in the NMR relaxation experiment[26,29]).

RESULTS AND DISCUSSION

1. Effect of Deprotonation of HIS48 on N-Terminal's Hinge-Loop. NMR titration experiment verified the existence of large conformational changes of RNase A accompanied by protonation/deprotonation process of histidine48. Here we performed MD simulation based on different protonation states of HIS48, namely, HIP48 (protonated), HID48 (deprotonated) (as labeled in Figure 2), as well as the mutated state H48A. We begin by examining how the structure and dynamics of RNase A change with the protonation state of HIS48 in MD simulation. The defined secondary structure of protein[31] (DSSP), which is commonly used to observe the time evolution of protein's secondary structures, is plotted along a 70 ns simulation period in Figure 3. The main difference observed in Figure 3a−c is the structure of the hinge-loop (residue 14 to 21), which connects the N-terminal helix and the helix-2. In the double protonation state (or positively charged state) HIP48, The HE2@HIS48 forms a stable hydrogen bond with the OG1@THR82 (hydrogen bond length:1.83 Å). The formation of this hydrogen bond brings stability to the local structure around the hinge loop and keeps its structural integrity over the course of MD simulation as shown in Figure 3a.

However, when the HE2@HIS48 is deprotonated or HIS48 is mutated to Ala, the above hydrogen bond disappears and the original interaction network around HIS48 is broken. As a result, residues around HIS48 relax to another stable conformation. The most noticeable change after this relaxation is that the hinge loop now forms a stable 3_{10}-helix structure as shown in Figure 3b,c. Previous experimental studies[11,20,21] suggested that the change of this hinge-loop structure plays a critical role in affecting the

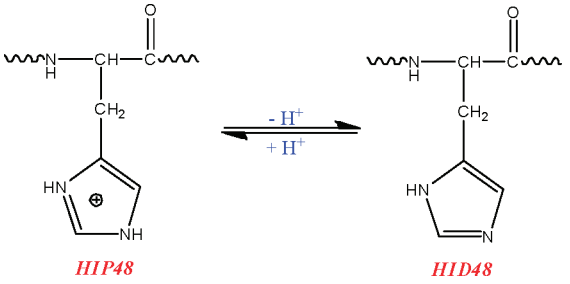

Figure 2. Chemical equilibrium between HIP48 and HID48 due to protonation of HIS48 (X-ray diffraction data of Rnase A at high pH shows that deprotonation occurs on HE2@HIS48[1]).

enzyme's catalytic dynamics, both local and global, as will be discussed below.

It is interesting to note that the partial denaturing of this hinge loop is also observed in other cases. By searching the Protein Data Bank, it is found that RNase-A can form a dimer using the domain swap mechanism.[32] The two monomers can dimerize through exchange of a N-terminal helix (residue 1−12) with the major domain (23−124) of the other subunit. As shown in Figure 4, conformations of the two hinge loops (14−21) that connect the N-terminal helix and the main domain are different. In particular, one of the hinge loops turns into a helix and the other becomes extended (highlighted by brown color in Figure 4).

It is useful to mention here that although the hinge-loop forms the helical structure in both HID48 and H48A, its impact on global and local enzyme dynamics (discussed below) is different in the two cases. These differences are likely responsible for the lower catalytic efficiency in the mutated RNase A relative to the wild type.[29]

2. Effect of Deprotonation of HIS48 on Enzyme's Global Dynamics. The enzyme's global dynamics is determined by protein's native structure and dynamic interactions among residues. From the result and analysis above, it is established that the structure of the N-terminal's hinge-loop of RNase A undergoes a change from the original loop structure to a 3_{10} helix due to depronation or mutation of HIS48. This local structural change, however, seriously affects the global dynamics of the enzyme. For this purpose, we analyzed dynamic cross correlations between residue pairs after the protein settled to its stable structure (after the first 10 ns simulation).

The cross correlation dynamics analyzed from 60 ns simulation time (after initial 10 ns) are plotted in Figure 3d−f as two-dimensional maps. Although the overall shapes of the cross correlation map of the three states (HIP48, HID48, H48A) of enzymes are similar because the majority of secondary structures remain stable, some pockets of the maps exhibit differences. The global picture of the heat (cross correlation) map is controlled by hot colors. The hot color denotes positive correlation reflecting the overall motion of the protein's secondary structures. For residue pairs belonging to the same sheet or helical structure, their motions are usually positively correlated. What is more interesting to us is the cold color which represents anticorrelated motion of residue-pairs. In HIP48, two most noticeable anticorrelated motions are those between the N-terminal helix and C-terminal sheets (circled purple box in Figure 3d) and between two wings around the binding pocket (central dark blocks in Figure 3d). These anticorrelated motions are illustrated in Figure 5a and b.

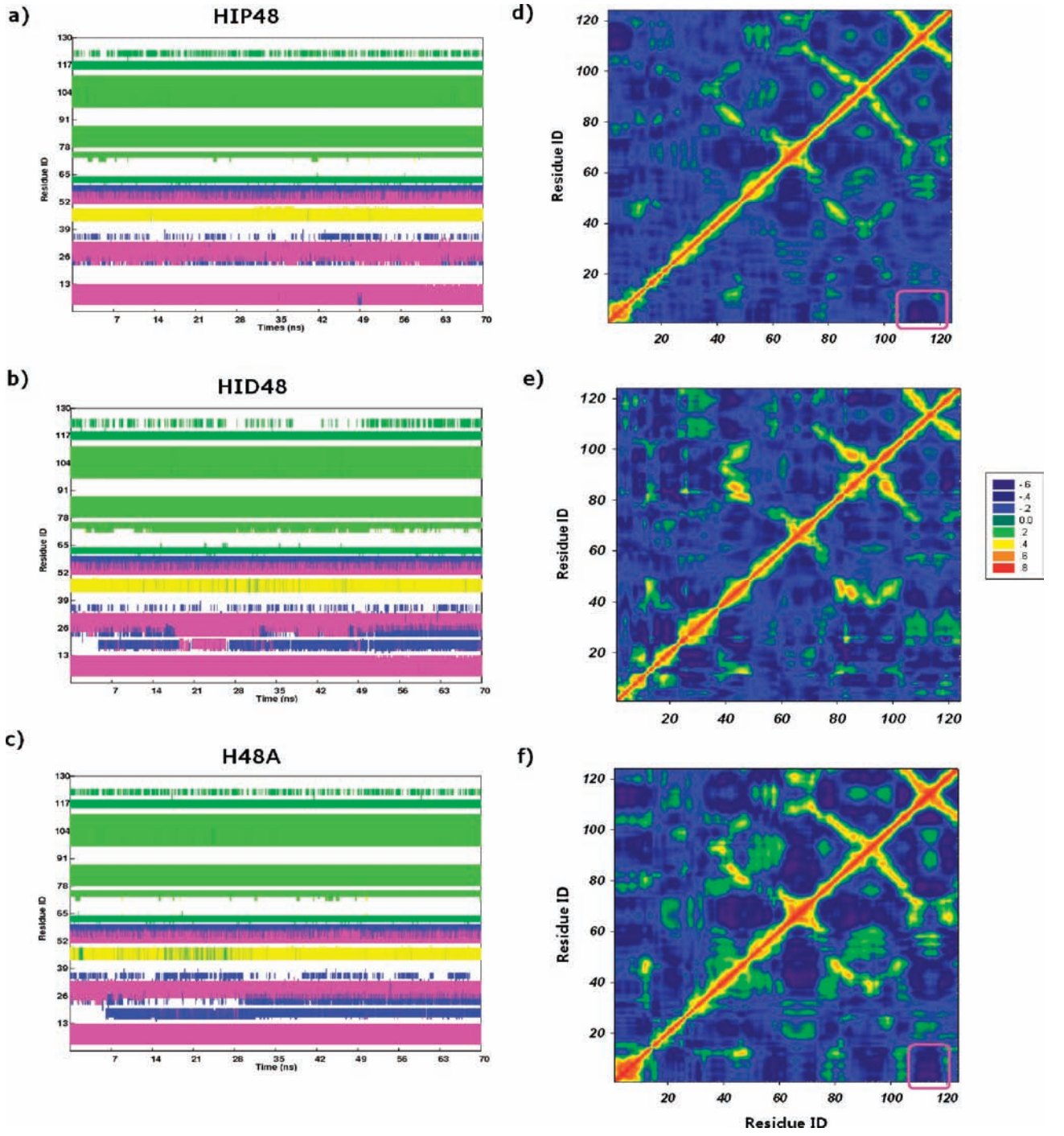

Figure 3. (a−c) Evolution of DSSP as function of simulation time for HIP48, HID48, and H48A, respectively (parallel sheet, red; mixed P/A sheet, yellow; double antiparalel sheet, purple; 3-helix, blue; 4-helix, green). (d−f) Heat map of correlations between each residue pair in HIP48, HID48, and H48A, respectively.

In the HID48 variant, most noticeable anticorrelated motion exists between helix-2 and the newly formed 3_{10}-helix (Figure 5c), which is different from that in HIP48 and H48A. Although the hinge-loop of HID48 also forms a rigid helical structure, its effect on global dynamical behavior is quite different from that in H48A. For example, if two domains are making some ordered anticorrelated motions, cold colors would be observed on the correlation map. In contrast, if two domains are making small energy adjustment or slowly drifting away from each other, the signals would be dominated by local random motion with little correlation. This seems to be the case in HID48, and it implies that the enzyme did not reach its equilibrium after deprotonation in the 10 ns simulation. It continues to make conformational adjustment from the initial structure in the following 60 ns simulation, which explains why the observed correlation map differs appreciably from that of HIP48. In particular, the missing signal due to the most visible anticorrelated motion between the N-terminal helix and C-terminal

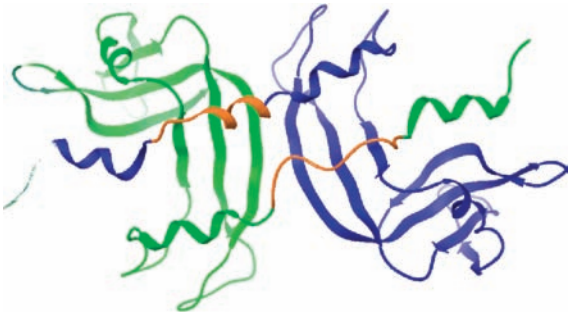

Figure 4. Structure of RNase dimer. Two hinge loops are highlighted in brown. (PDB ID:1A2W[19].)

sheets indicates that rearrangement of the relative position between the N-terminal helix and main-domain of the enzyme occurs after deprotonation of HIP48. This phenomenon observed in MD stimulation of the HID48 variant is consistent with the experimental observation that partial unfolding of the N-terminal helix is the precondition for the formation of dimer structure.[32,33]

The above result clearly shows that the change of protonation state of RNase A triggers enzyme's local conformational change, which further affects large scale interdomain motions. Since enzyme's interdomain correlated motions are different between HIP48 and HID48, relaxation time detected from NMR experiment should be different. Thus, two signals should be detected from NMR experiments that correspond to two different structures of RNase (HIP48 and HID48). Of course, relative intensity of the signal will be dependent on the acidity of the system. The current simulation result of the two protonation states of RNase A is in excellent agreement with previous experimental observations using biochemical methods and NMR relaxation techniques.[29]

Here we summarize some experimental observations and theoretical findings: (1) Discontinuity of titration curve of HIS48 implies that large conformational change occurrs during the depronation process of HIS48.[19−23] (2) NMR relaxation experiment verified that the protonation state of HIS48 controls the conformational change of RNase A.[6,25−29] (3) Our simulation shows that the hinge region of HID48 undergoes similar conformational change as that in the dimer. (4) Depronation of HIP48 causes rearrangement between the N-terminal helix and C-terminal sheets. (5) Experiments found that partial unfolding of the N-terminal helix is the precondition for the formation of dimer structure.[32,33] The above experimental and theoretical findings strongly suggest that new interaction networks (see sections 3 and 5) in HID48 drive the N-terminal helix to change its conformation slowly. Such conformational change may occur in microseconds to milliseconds.[6,29]

3. Perturbation Study of Large Scale Enzyme Motions. To find further evidence of this mechanism, we employed a perturbation method to explore large scale motions in RNase A. Since large scale protein motions are beyond the reach of routine MD simulation due to time limits,[34] we applied RIP (rotamerically induced perturbation) method by Ho and Agard[35] to probe the flexibility of large conformational changes in RNase A. In the RIP method, torsional perturbation is applied to individual side chains in the MD simulation, and this can generate large, coherent motions of structural elements in picoseconds. The RIP method has been successfully applied in predicting many

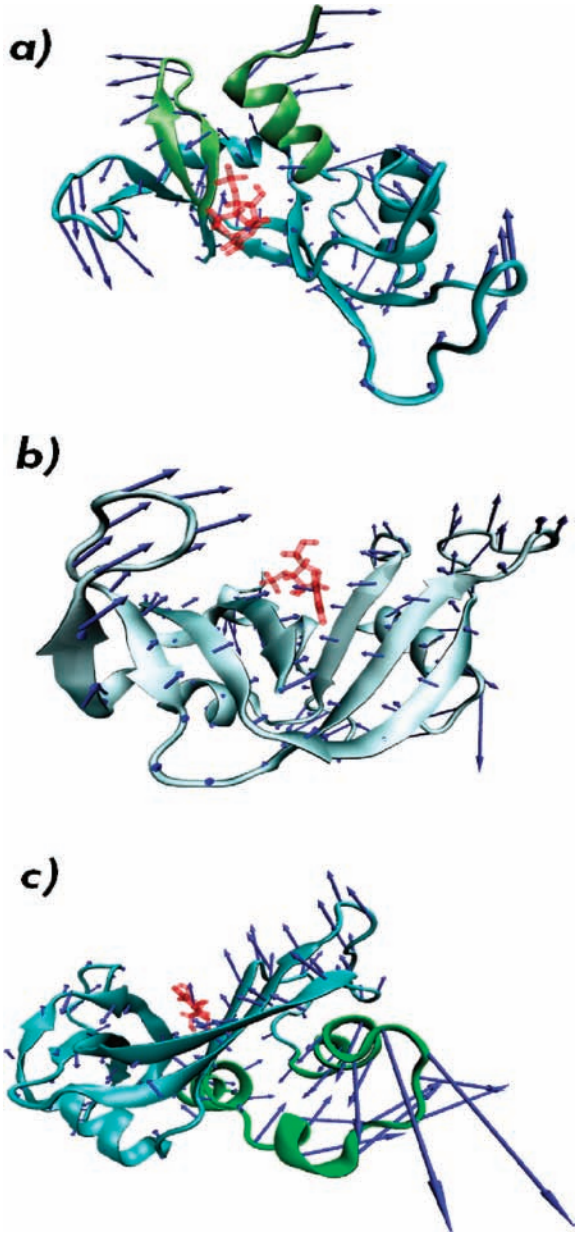

Figure 5. Three most important vibrational modes: (a and b) in HIP48 and (c) in HID48. These are dominant vibrational modes uncovered from PCA analysis.

important functional motions in proteins.[35] In the current RIP application, the final structure from the explicit water MD simulation is used as the reference structure and all rotatable side chains are examined. The calculation shows that the N-terminal helix-1 slowly leaves the protein body when Met13 is perturbed in the HID48 state. This implies weakened connection between the N-terminal helix-1 to the main-domain. This phenomenon, however, is not observed in the protonated state HIP48 and the mutant H48A. (movies available in the Supporting Information)

Whether HIP48 is deprotonated into HID48 or mutated into H48A, the native interaction network established around Histidin 48 is broken and a new equilibrium between intraprotein and protein-water interactions is established. In order to understand different dynamical behavior observed in the RIP

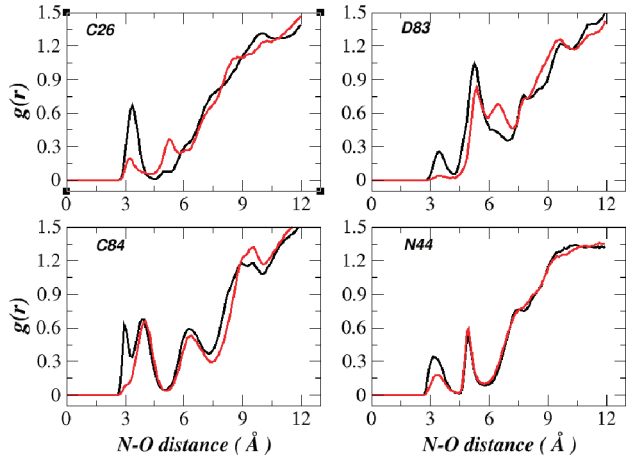

Figure 6. Radial distribution function of the solvent around backbone N atom in each residue. (black, HIP48; red, H48A.)

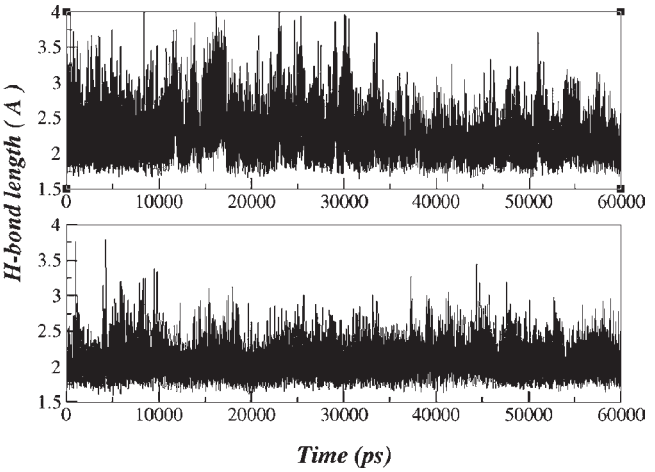

Figure 7. Time evolution of backbone hydrogen bond length between residue C84 and N44 in HIP48 (top) and H48A mutant (bottom).

study, Hydrogen bonding between the N-terminal helix-1 and the other parts of the protein is analyzed. There are, respectively, eight, six, and nine hydrogen bonds in HIP48, HID48, and H48A. (Detailed hydrogen bond interactions are listed in Table S1 in the Supporting Information.) Thus deprotonation caused reduction of two hydrogen bonds in HID48, which explains why the N-terminal helix of HID48 can move away from the main-domain more easily. This conformational flexibility may facilitate the release of the catalytic product (see SMD simulation in section 8).

It is important to note that the interface between the N-terminal helix and the main domain is the only hydrophilic interface in RNase A. Because hydrophilic interfaces are more susceptible to solvent effects than hydrophobic interfaces,[36] they are capable of exercising large scale dynamical motions with specific functions. The relationship between protein's large scale dynamics and function has attracted much research interest in recent years.[4,37−43] The present study of RNase A demonstrates that studying those hydrophilic interfaces can help our understanding of protein's functional dynamics.

4. Local Dynamics at Active Site. Both the local structure and dynamics of H48A mutant are different from those of HIP48. In the following, local dynamic motion of some special residues around the ligand-binding pocket is analyzed. For residues exposed to solvent, their dynamic motions can often be inferred from the behavior of the solvent molecules around them. For example, the radial distribution function of solvent molecules around the backbone N atoms of specific residues can be a useful indicator on enzyme's local dynamics. Figure 6 shows plots of radial distribution functions around selected residues that are on the same wing as the mutational site in both HIP48 and H48A mutant, respectively. Important difference in radial distribution function is observed in Figure 6. C26, D83, C84, and N44 were all part of helical or β-sheet structures, and all NH groups of these four residues form standard backbone hydrogen bonds with the CO groups in the protein. The RDF (radial distribution function) pictured in Figure 6 reflects the distribution of water molecules around the backbone amide N atom of each of these four residues. The first RDF peak in Figure 6 represents the direct hydrogen bond interaction between NH of each residue with water molecules. In the HIP48 state, the first peak was relatively higher than that in the H48A mutant. This means that

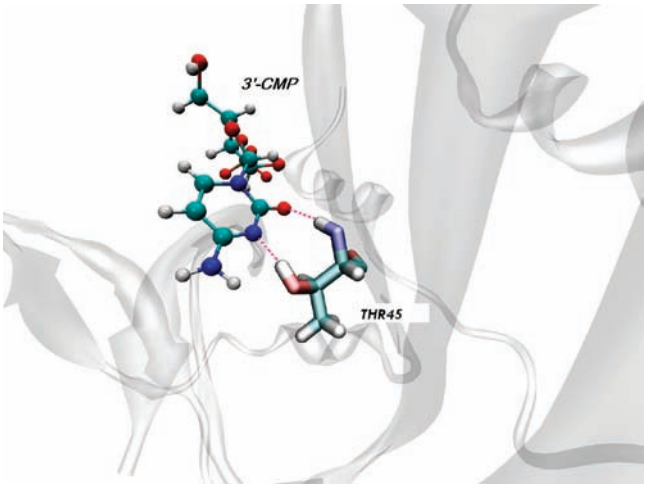

Figure 8. Relative position between THR45 and 3′-CMP.

these NH groups in the HIP48 state are more accessible to water molecules and the backbone hydrogen bonds were not as stable as in the H48A mutant (see Figure 7). For residues C26, C84, D83, and N44, there are more water molecules in the first solvation shell in the HIP48. This observation indicates that these residues around the active site in the wide type are more flexible and therefore more accessible to the surrounding waters than those in the mutant. This rationale is supported by further analysis in Figure 7 which shows the comparison of time evolution of the related hydrogen bond length in the HIP48 and the mutant H48A. As shown in Figure 7, the time evolution of the backbone hydrogen bond between residues 84 and 44 is indeed more stable in the H48A mutant than in the HIP48.

HIS48 is a critical bridge that connects motion of the N-terminal hinge (res 14−21, far away from the active site) and motions of residues around the active site. Once HIS48 is mutated, residues around the ligand all stay in some "ground state". For residues on the other side of the protein, especially for residues on loop-4 (A64, K66, Q69, N71), no significant differences in the solvent's RDF were observed (see Figure S1 in the Supporting Information). This is in good agreement with the experiment on solvent kinetic isotope effect. As pointed by

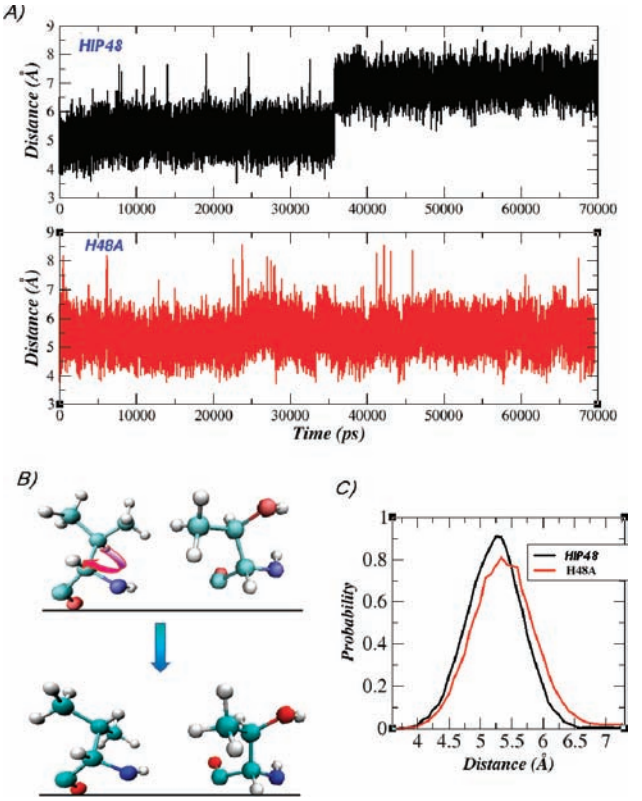

Figure 9. (a) Distance between CG@THR45 and CG1@ILE47. (b) Rotation of the side chain of ILE47. (c) Distribution of the distance before rotation of the side chain.

Watt and co-workers, mutation on H48 has no effect on relaxation dynamics of residues involved in loop-4.[26,29]

Here we analyze some detailed dynamic information on one specific residue in the active site, THR45 (Figures 8 and 9). THR45 forms two hydrogen bonds with the catalytic product, which is recognized as the most important interaction between the ligand and the enzyme. The methane group of THR45 is in contact with ILE47 directly through van der Waals interaction. Due to the excess energy in HIP48, the side chain of ILE47 is forced to rotate after about 35 ns. We can imagine that, in the HIP48 state, the motion of the hinge correlates with the motions of residues around the ligand through the bridge residue HIS48. Thus, more vibrational energy is transferred through the HIS48 and other protein networks in which the hydrogen bonds serve as the building blocks.

The generalized order parameters (S^2) of the NH vector in each residue are usually used in charactering a protein's dynamic personality[44−46] in NMR experiments. The S^2 represents dynamic flexibility of each residue of the protein. Generalized order parameters of each residue in the HIP48 and H48A mutant were analyzed. From Figure S4 in the Supporting Information, we find that the order parameter of NH@THR45 is lower in the HIP48 state than in the H48A mutant. This suggests that the dynamic motion of THR45 is more vigorous in HIP48 than in H48A. Although we did not observe the breaking of hydrogen bonds between THR45 and the ligand (catalytic product) during our simulation study, a more energetically charged THR45 and other more flexible residues around the activation pocket in HIP48 may facilitate the release of the final product from the enzyme.

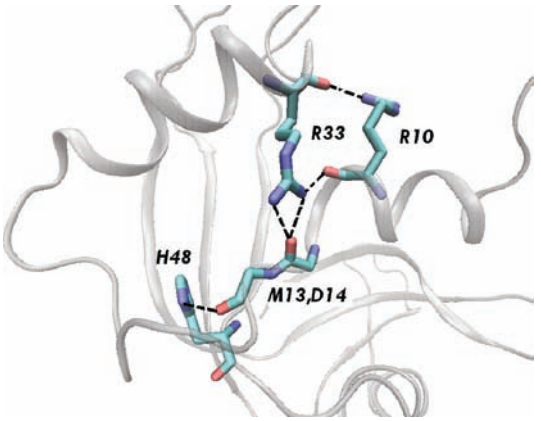

Figure 10. Hydrogen bond network that connects H48 with the N-terminal helix-1. For clarity, only the backbone atoms of Met13 and D14 are shown.

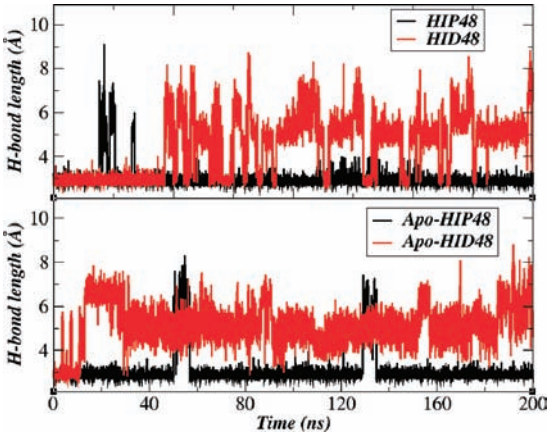

Figure 11. Time evolution of the hydrogen bond length between NH1@Arg33 and O@Arg10 in four separate MD simulations.

5. Deprotonation of HIP48 Partially Disrupts the Interaction Network Between Helix-1 and the Main Domain. The crystal structure[47] shows that strong interaction exists between Arg33 of the main-domain and Arg10 in N-terminal helix. The side chain of Arg33 forms a hydrogen bond with Arg10's backbone C═O group while the side chain of Arg10 forms a hydrogen bond with Arg33's backbone C═O group. The Arg33's large hydrophilic side chain is also involved in hydrogen bond networks formed by residues of loop-1. In addition, HIS48's side chain is also involved in this interaction network (see Figure 10). This kind of relationship makes it possible that changing HIS48's protonation state may result in rearrangement of the original hydrogen bond network around loop-1 and further influence Arg33's interaction with Arg10.

Here we extend our simulations for HIP48 and HID48 to 200 ns each to explore the relationship between the protein stability and interdomain interactions. Since the functional dynamics exists in both the apo- and substrate bounded form, dynamic personalities of apo-HIP48 and apo-HID48 are also studied for comparison. The hydrogen bond length between the side chain of Arg33 and C═O of Arg10 is plotted in Figure 11. This figure shows that this hydrogen bond breaks frequently in both apo- and substrate bounded HID48 form. However, the same hydrogen bond is well preserved in HIP48. Since the protein's 3D

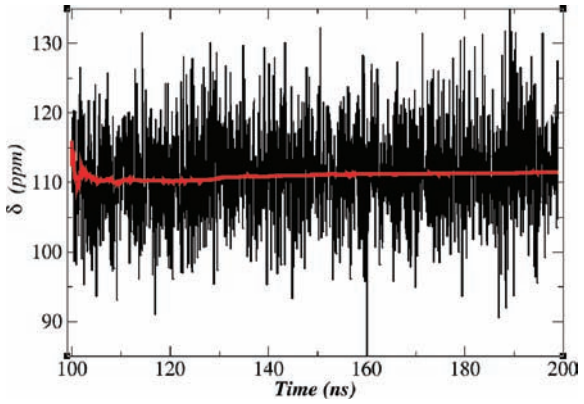

Figure 12. Calculated ^{15}N chemical shift of H12 in apo-HID48 as a function of simulation time. The red line is the time-averaged value of chemical shift.

structure is determined by a delicate balance among all kinds of intraprotein and protein−water interactions, a small perturbation of a local interaction could result in large scale conformational change.

Not only backbone hydrogen bonds but also side chain hydrogen bonds contribute to the helix's stability. In early studies, the N-terminal of RNase-A was used as a model system to study the energetics of protein folding.[48] Brown and Klee[49] have found that only marginal helical conformation was detected from the isolated N-terminal helix of RNase A. The experiment of Brown and Klee suggested that interactions between the N-terminal helix and other parts of the protein including the interaction between Arg33 and Arg10 are also important in preserving helix-1's stability. Deprotonation of HIP48 disrupts the original interaction network around loop-1 and causes chain reactions. For example, the N-terminal helix becomes destabilized after breaking of the interaction between the N-terminal helix and the main domain of RNase A (see discussions in sections 3 and 7). Since the N-terminal helix is one of the building blocks of the substrate binding pocket and many side chains of helix-1 interact with the catalytic product directly, destabilization of helix-1 can facilitate the release of the product from the catalytic center.

6. Calculation of Chemical Shifts. Since NMR chemical shift is very sensitive to the chemical environment, it is widely used to extract information about a protein's structure and dynamics.[44,46,50] The experimental study of Watt et al.[29] observed a change of chemical shift for some residues in Rnase A before and after the ligand binding. The change of chemical shift of the N atom of the amide group in H12, A19, and K31 was measured to be about −0.8, −0.5, and 0.4 ppm, respectively, in the wild type. We note that these values of changes in chemical shift are well within the error bars of theoretical calculations.[51] This is demonstrated from our calculation of chemical shifts for these three residues. First, the protein system is too large for any standard quantum chemistry calculation of chemical shift. Only a smaller subsystem is used to perform the calculation in the QM/MM approach. Second, the ab initio calculation of the chemical shift for amide nitrogen has inherent error that is much larger than the experimentally measured values (less than 1 ppm) here. Finally, the force field used to perform MD simulation also contains errors that cause inaccuracy in structural distribution of the protein. Thus, obtaining a quantitative or even qualitative comparison of chemical shift changes between the theory and experiment is not very realistic in the present case. Nevertheless, it is certainly worth the effort to try, and we thus performed QM/MM calculation to compute these chemical shifts. Since the calculated chemical shift $\delta(N^{15})$ fluctuates wildly, the final result was obtained by averaging over 2000 snapshots as shown in Figure 12. This shows that calculation of the chemical shift at a single geometry is not very meaningful.

Table 1. Calculated Chemical Shift of ^{15}N for Three Residues in Apo- and Complex States of RNase A[a]

	HID48 apo	HID48 bounded	HIP48 apo	HIP48 bounded	Δ
H12	111.5	114.9	109.1	110.9	−0.6
A19	113.9	113.9	111.6	111.8	−2.1
K31	114.7	116.5	115.8	115.9	1.2

[a] The change of chemical shift is given by $\Delta = \delta_{bound}(\text{HIP48}) - \delta_{apo}(\text{HID48})$.

The calculated chemical shfit δ (N^{15}) and its change ($\delta_{bound} - \delta_{apo}$) in apo- and complex states are listed in Table 1. In view of the fact that the inherent error of the theoretical calculation is much larger than the experimental values for the current systems, the qualitative agreement with the experimental data in the change of chemical shift for the wide type RNase A is encouraging.

7. Longer Time Dynamics of Apo-RNase A (HID48 variant). From the analysis of correlated dynamics and possible large scale motions of RNase A in different states in previous sections, we found that the HID48 is mostly responsible for RNase A's functional dynamics related to the product release. In order to further explore the detailed relationship between the dynamics of loop-1 and of the binding pocket, we choose to simulate longer time dynamics of the apo-form (0.75 μs simulation on Apo-RNase A (HID48)). It was recognized that functional dynamics exists in both the apo- and substrate bounded states and the former is more flexible than the latter. In order to extract more information from the limited computational resources, we chose to simulate longer time dynamics of the apo-state.

The information derived from the nanosecond dynamic simulation may contain local random motion, which can be averaged out in longer time simulation. Global or long-range domain−domain coupled motion may be captured by longer time scale dynamics simulation. How the flexibility of loop-1 influences the dynamics of other part of the protein at the microsecond time scale is what we are interested in.

Similar dynamical correlation map of the Apo-RNase (HID48) constructed from the 0.75 μs MD trajectory is plotted in Figure 13a. By focusing on loop-1 (residues 14−21), we find four major hot spots. To pick out residues that have strong dynamical correlations with loop-1, correlation maps associated with two representative residues (16 and 18) are projected out and plotted in Figure 13b. Four highly correlated spots are marked in Figure 13b. The highest peak comes from the strong dynamic correlation between the neighboring residues in loop-1 and is not marked. The peak-I in Figure 13b represents strong correlation between loop-1 and loop-2 (both are connected by helix-2). It is not surprising to see that their dynamic motions are strongly correlated. Peak-II in Figure 13b represents sheet β-1 (residues 41−49) which is located in the core region of the binding pocket, and many of its residues interact with the substrate directly through hydrogen bonding. Since loop-1 is

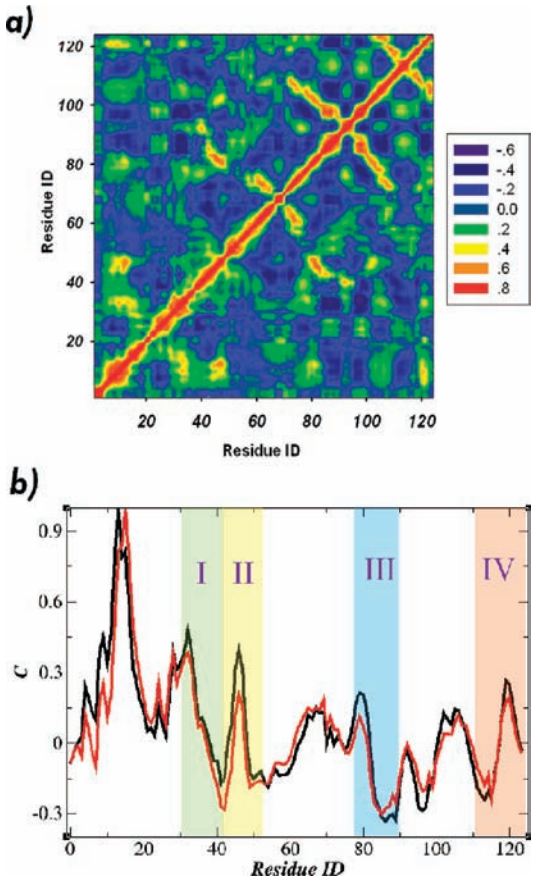

Figure 13. (a) Heat map of correlations between each residue pair in Apo-Rnase A (48HID). (b) Correlations of two standard residues in loop-1 (black, residue 16; red, residue 18).

located 15 Å away from the catalytic center, the observed significant correlation of dynamic motion between loop-1 and sheet β-1 suggests that dynamic energy of long-range loops can be transferred into the catalytic pocket efficiently. What's more interesting to us is that residue THR45, as mentioned in the fourth section, has the highest correlation value among other residues in sheet β-1. Residue THR45 makes a substantial contribution to the binding of the product by forming two hydrogen bonds with it. From Figure 13a, we find that correlations between residues around THR45 and resides of Loop-1 are the highest besides those in the secondary structures, that is, residues in the same helix or β sheet. The picture shown in Figure 13a may reflect how robust the protein's three-dimensional networks are in maintaining an enzyme's catalytic efficiency. Similar strong correlation is also observed in sheet β-4 as inferred from peak-III. Sheets β-1, β-4, and β-5 form an integral network that can facilitate transfer of dynamic energy of the flexible loops to the catalytic center and further help release the catalytic product. After chemical reaction is completed, this well organized β-sheet network acts as an energy transporter to transfer dynamic energy of loop-1 and other flexible residues that are far away to the reaction center. This efficient network for transferring dynamic energy may facilitate the release of the catalytic product.

After scanning the time evolution of the secondary structure of Apo-RNase A (HID48) with DSSP procedure (see Figure S2 in the Supporting Information), we found that the loop-1 forms a

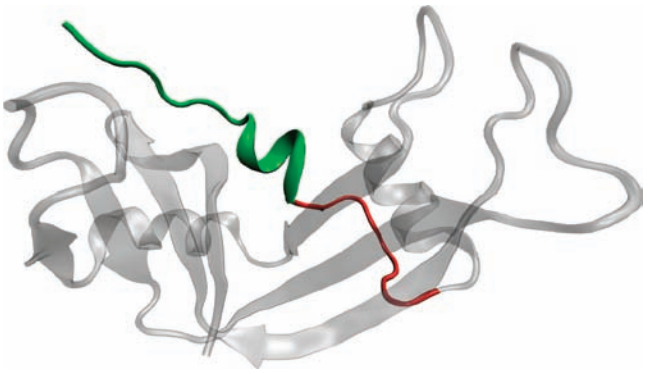

Figure 14. Final structure of Apo-Rnase A (HID 48) after 0.75 μs MD simulation. Original helix-1 is highlighted with green color, and loop-1 is highlighted with red color.

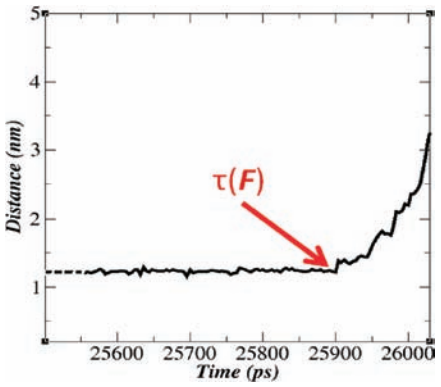

Figure 15. Time evolution of the distance between the fixed point (atom) in the protein and the point (atom) in the ligand where external force (F = 500 pN) was applied in SMD simulation of the HIP48 state.

partial 3-helical conformation in one-third of all the simulation time and the N-terminal helix unfolds partially. The final structure of Apo-RNase A after 0.75 μs time simulation is plotted in Figure 14. This observation is consistent with our findings in previous sections using the RIP method. Since helix-1 is the integral part of the substrate binding pocket, the result suggests that increased flexibility of the N-terminal helix in the HID48 state is important in enhancing RNase A's catalytic function by speeding up the release of the product.

Rearrangement of local hydrogen bond networks around loop-1 due to deprotonation of HIS48 results in weaker interaction between helix-1 and the main domain, for example, by breaking the hydrogen bond between Arg33 and Arg10 of helix-1. Weakened interaction between the N-terminal helix and the main domain makes the N-terminal helix more flexible. A more flexible N-terminal helix can loosen the binding between the enzyme and the product.

8. Mechanical Stability of Rnase A/Ligand Complex. It is known from the analysis in section 5 that the local interaction networks around the ligand binding pocket differ substantially in different protonation states of HIS48, especially for hydrogen bonds related to the N-terminal helix-1. The binding pocket was relatively lossened in HID48 compared to that in HIP48. Steered molecular dynamics (SMD) has been widely used for studying protein−ligand binding and a protein's mechanical stability extensively.[52−56] Previous SMD predictions agree well with

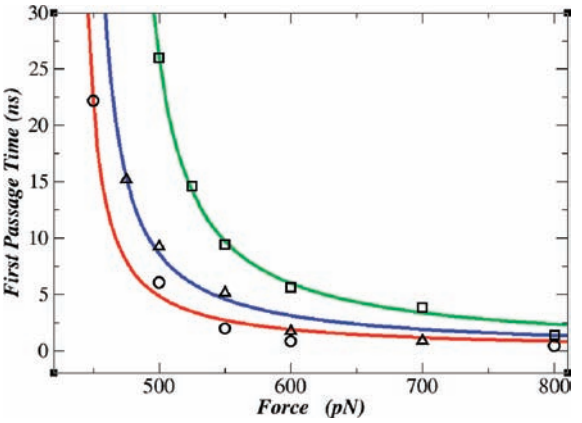

Figure 16. First passage time versus applied external force for HIP48 (box and green line), HID48 (circle and red line), and H48A (triangle and blue line). Curves are fitted according to eq 1.

atomic force microscopy (AFM) observations.[57] SMD provides a simple protocol in probing a protein's mechanical stability and protein−ligand binding strength.[57] Here we explore the mechanical stability of Rnase A/ligand by performing the constant force SMD simulations.

In SMD simulation, one point on the protein was fixed and an external force was applied to a point on the ligand to pull the ligand away from the protein. One trajectory is pictured in Figure 15. Figure 15 shows that the complex preserves its stability until 25.9 ns which was the duration time of HIP48 state under 500 pN. Under different forces, the duration time probed by SMD is different. A simple way to connect duration time with effective potential barrier of the protein−ligand unbinding process was built up on the mean first passage time theory[54,55,58−60] by Schulten and co-workers.

$$\tau(F) = 2\tau_d{}^2\delta(F)^{-2}[e^{\delta(F)} - \delta(F) - 1] \quad (1)$$

where $\delta(F) = \beta[\Delta U - F(b - a)]$. Equation 1 connects the mean first passage time of interest, $\tau(F)$, with the external force applied, F. In eq 1, F is externally applied, $\tau_d = (b - a)/2D$, where $(b - a)$ is the barrier width of the potential (~3.0 Å), and D is the effective diffusion constant. Thus, we can obtain parameters ΔU and D through fitting curves with points derived from SMD simulation. The numerically fitted barrier height is 20.4, 18.5, and 19.2 kcal/mol, respectively, for HIP48, HID48, and H48A.

The results presented here provide a qualitative view on the rate of protein−ligand unbinding in different states. The first passage time in Figure 16 shows that ligand unbinding is the fastest in the HID48 state and the slowest in the HIP48 state. The result in Figure 16 supports our theoretical model in which the HID48 is the "open" state for product release and is thus consistent with the experimental finding that product release is the rate determining step in the catalysis of RNase A. This result may also support the hypothesis that state transformation is essential for the wild type Rnase A be catalytically robust. However, one needs to keep in mind that SMD may only capture the influence of nearby structure differences around the ligand. Dynamical coupling effect of reaction center and the hinge loops far away from the binding pocket could not be captured in this SMD simulation.

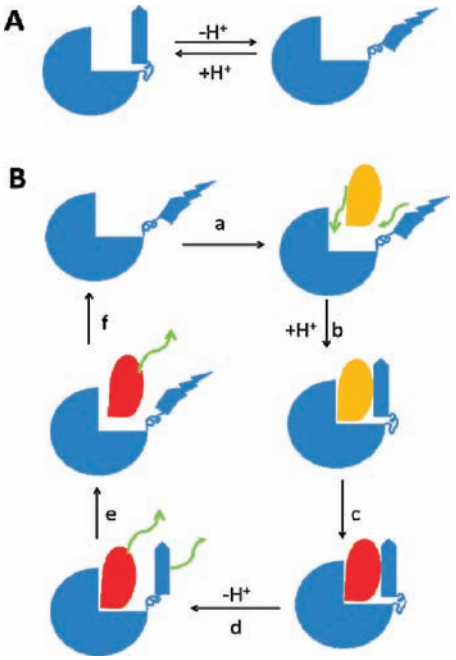

Figure 17. (A) Schematic illustration of the conformational change due to protonation/depronation of His48. (B) Schematic illustration of mechanism proposed on how changing of protonation state of His48 enhances catalytic power of Rnase A. (a) Recruiting of the RNA substrate in the open state. (b) After binding with the substrate, the closed state (protonated HIS48) becomes more stable. (c) Chemical reaction occurs in the closed state. (d) After the catalytic process, depronation of His48 introduces partial drifting of the N-terminal helix which facilitates the release of the catalytic products.

CONCLUSION AND DISCUSSION

Based on previous experimental studies[4−6,11,21,29] and our theoretical understanding, a schematic illustration of how protein's structure and dynamics control RNase A's catalytic power is shown in Figure 17. In physiological conditions, RNase A adopts two conformations that correspond to closed (HIP48) and open (HID48) states that coexist depending on the protonation equilibrium of His48 (Figure 17A). When RNase A is in the open state (HID48), it is relatively easier to recruit the RNA substrate (Figure 17B.a). Binding of the substrate energetically favors the closed state due to the bridging effect of the ligand and stabilizes the protonated form of HIS48 (Figure 17B.b). Chemical reaction occurs in the closed state with the help of HIS12 and HIS119 (Figure 17B.c). After the reaction is completed, deprotonation of His48 drives the partial unfolding of the N-terminal helix and facilitates the release of the catalytic product (Figure 17B.d). After releasing the product, RNase A returns back to the apo-state.

The dynamical mechanism for the above process is proposed as follows: In the "closed" state HIP48, the N-terminal's hinge loop is intact and the enzyme remains in a relatively stable conformation, which is preferred for catalytic reaction to take place. After the chemical reaction is completed, deprotonation of HIS48 occurs and this induces the denaturing of this hinge-loop into a more energetically favorably 3-helix (see Figure S3 in the Supporting Information), causing it to break the original interaction network around loop-1 and drive the partial unfolding of the N-terminal. This correlated dynamic motion facilitates the

release of the catalytic product, which is the rate determining step, and therefore helps speed up the overall catalytic process.

Here we summarize some important insights derived from MD simulation in combination with the available experimental observations. The deprotonation of His48 in RNase A controls the functional motions in this enzyme. In the double protonation state HIP48, the N-terminal helix (part of the binding pocket) is stable. Deprotonation of HIS48 from HIP48 to HID48 is accompanied by large conformational change. For example, deprotonation of HIP48 interrupts the original hydrogen bond network around loop-1. One important role of HIS48 played in RNase A's catalytic cycle is uncovered in the current study. His48 acts as a modulator for transformation of conformational state through perturbation of hydrogen bond networks across loop-1, N-terminal helix, and other residues nearby. Our study also suggests a possible role played by His48 to transport loop-1's kinetic energy to the reaction center.

Protonation and deprotonation of His48 occur in milliseconds in physiological conditions. The rate of the protonation/deprotonation process and the relative distribution of two protonation states are strongly influenced by the pH value of the system. In the HID48 state, the N-terminal helix is relatively flexible compared to that in the HIP48 state. Since catalytic chemical reaction prefers a relatively stable transition state, the stable HIP48 state is preferred for this purpose. On the other hand, a more flexible HID48 form is preferred for product releasing process. Thus, there is a need for state transformation of RNase A in order to complete the entire catalytic process efficiently. As a result, the process of state transformation between HIP48 and HID48, which occurs in the millisecond time scale, becomes the bottleneck of the catalytic turnover process. This proposed scenario is compatible with the available experimental observations.[4−6,11,21,29]

METHODS

Molecular Dynamics Simulations. In this study, the crystal structure of RNase A complexed with 3′-CMP determined by Zegers et al.[47] is used as the starting structure (PDB ID: 1RPF). MD trajectories are generated for the following states: (1) Both nitrogen atoms of the indo group of HIS48 are protonated (HIP48). (2) Only one of the nitrogen atoms is protonated (HID48). (3) HIS48 is mutated to alanine (H48A). Hydrogen atoms are added according to each residue's standard protonation state. Also, all other histidine side chains are protonated according to their local environment (protonated on N^{δ}@HIS105,119; $N^{\varepsilon}$and N^{δ}@HIS12). The enzyme is solvated in an octahedron-like TIP3P water box, and the system is neutralized by adding counterions. Periodic boundary conditions and the particle mesh Ewald methods are used to treat long-range electrostatic effects. Each system is relaxed in 5000 steps with constraint on protein, followed by full minimization without any constraints. For MD simulation, integration time step is 2 fs. Temperature is regulated using Langevin dynamics with the collision frequency set to 2 ps^{-1}. All the covalent bonds involving hydrogen atoms are fixed by applying the SHAKE algorithm. After heating and equilibration, the production MD simulation is performed at 300 K and 1 MPa (NPT). For protein, the Amber99SB force field[30] is used in the simulation. For the ligand, Amber GAFF parameters are used. The intermediate structures are saved every picosecond for analysis. Amber10 software[61] was used in all the MD simulations. A PYTHON wrapper (downloaded from Ho's website[62]) and sander package of AMBER were used for the RIP simulation. For the RIP simulation, ligand and waters are removed. The simulation was conducted with the GBSA implicit solvation model with the Amber parm96 force field. To explore possible large scale motions in protein, perturbation force was added on the side chain of the selected residue. All rotatable side chains are examined in the current study. Details of the RIP simulation method can be found in the original paper of Ho and Agard.[35]

Structure and Correlation Analysis. Ptraj[61] module of Amber Tools software was used for hydrogen bond analysis and principle component analysis (PCA). Correlated motions are extracted from dynamic cross-correlation maps. The cross-correlation coefficient for each pair of C-alpha atoms i and j is given by

$$C_{ij} = \frac{\langle \Delta r_i \Delta r_j \rangle}{\sqrt{\langle \Delta r_i^2 \rangle \langle \Delta r_j^2 \rangle}}$$

where Δr_i is the displacement from the mean position of the ith atom and the symbol $\langle\rangle$ represents time average over the MD trajectory.

Quantum Mechanical Calculation of Chemical Shifts. All electronic structure calculations were performed using the density functional theory of M06/6-31G** implemented in Gaussian09 software.[63] Gauge invariant atomic orbital (GIAO) model[64] was used in calculating chemical shielding tensors. Isotropic chemical shifts are related to the shielding by a reference shielding σ_{ref},

$$\delta = \sigma_{ref} - \sigma$$

Systematic fit to experimental chemical shifts was desired to obtain the reference shielding. Here we only care about difference in chemical shifts between apo- and bounded states of RNase A

$$\Delta = \delta_1 - \delta_2 = (\sigma_{ref} - \sigma_1) - (\sigma_{ref} - \sigma_2) = \sigma_2 - \sigma_1$$

The chemical shift change is not related to the reference shielding. Here we calculate shielding of the NH_3 molecule as the reference (σ_{ref} = 258.2 ppm). Since the protein is too large for full system quantum mechanical calculation, a combination of quantum mechanical and molecular mechanical potential[65] was used for chemical shift calculation. The specific residue and its neighboring groups were treated with the QM method, while other parts of the protein and solvent molecules were treated as background charge (electrostatic embedding). Here we calculate chemical shifts of the amide N atoms of three residues of RNase A. A previous study[51] suggested that the hydrogen bond is very important in determining the chemical shift for amide N atoms in protein. It is thus important to include the NH group's hydrogen bond partner in the QM system.

The chemical shifts of three amide N atoms in H12, A19, and K31 were calculated here. Since the protein's backbone hydrogen bond fluctuates, the NH group may form hydrogen bonds with water in some snapshots. Two nearest water molecules around the NH group were also included in the QM system. A sample QM system is shown in Figure S5 in the Supporting Information. Since residue A19 is located in the hinge loop, the NH group of A19 can only form hydrogen bonds with water. We thus choose to include the five nearest water molecules in the QM system. A total of 2000 snapshots were extracted from MD trajectories (trajectory time period: 100−200 ns) for each chemical shift calculation.

Steered Molecular Dynamics Simulations. SMD simulation[55,57] was employed to probe the mechanical stability of the Rnase A/ligand complex under external force. The final structure from the 200 ns MD simulation in each state was used as the starting structure for SMD simulation. Forced unbinding was accomplished by adding a constant force to the N1 atom on the ligand while keeping the C_α atom of ILE47 fixed. Forces were applied along the vector connecting these two atoms ranging from 450 to 800 pN for each of the three complexes. The barrier height for the unbinding, ΔU, is determined from eq 1[55,59] by using a weighted least-squares fit with a barrier width of 3.0 Å, and the plateau duration was used as a measure of mean first passage time.

■ ASSOCIATED CONTENT

Supporting Information. Movies of RIP simulations; Figure S1−S5; Table S1 and complete list of authors of reference 63. This material is available free of charge via the Internet at http://pubs.acs.org.

■ AUTHOR INFORMATION

Corresponding Author
chicago.ji@gmail.com; john.zhang@nyu.edu

■ ACKNOWLEDGMENT

We thank the National Natural Science Foundation of China (Grants No. 21003048, 10974054, and 20933002) and Shanghai PuJiang program (09PJ1404000) for financial support. C.G.J. is also supported by "the Fundamental Research Funds for the Central Universities" and Open Research Fund of the State Key Laboratory of Precision Spectroscopy, East China Normal University. We also thank the Computational Center of ECNU for providing computational time.

■ REFERENCES

(1) Berisio, R.; Lamzin, V. S.; Sica, F.; Wilson, K. S.; Zagari, A.; Mazzarella, L. *J. Mol. Biol.* **1999**, *292*, 845.
(2) Raines, R. T. *Chem. Rev.* **1998**, *98*, 1045.
(3) Marshall, G. R.; Feng, J. A.; Kuster, D. J. *Biopolymers* **2008**, *90*, 259.
(4) Hammes, G. G. *Biochemistry* **2002**, *41*, 8221.
(5) Hammes, G. G.; Roberts, P. B. *J. Am. Chem. Soc.* **1969**, *91*, 1812.
(6) Loria, J. P.; Berlow, R. B.; Watt, E. D. *Acc. Chem. Res.* **2008**, *41*, 214.
(7) Brünger, A. T.; Brooks, C. L.; Karplus, M. *Proc. Natl. Acad. Sci. U.S.A.* **1985**, *82*, 8458.
(8) Merlino, A.; Vitagliano, L.; Antoine Ceruso, M.; Di Nola, A.; Mazzarella, L. *Biopolymers* **2002**, *65*, 274.
(9) Merlino, A.; Vitagliano, L.; Ceruso, M. A.; Mazzarella, L. *Biophys. J.* **2004**, *86*, 2383.
(10) Nadig, G.; Vishveshwara, S. *Biopolymers* **1997**, *42*, 505.
(11) Hammes, G. G. *J. Biol. Chem.* **2008**, *283*, 22337.
(12) Carty, R. P.; Hirs, C. H. W. *J. Biol. Chem.* **1968**, *243*, 5254.
(13) Eftink, M. R.; Biltonen, R. L. *Biochemistry* **1983**, *22*, 5123.
(14) MacKnight, M. L.; Spikes, J. D. *BioSystems* **1972**, *5*, 20.
(15) Matthew, J. B.; Richards, F. M. *Biochemistry* **1982**, *21*, 4989.
(16) Matthew, J. B.; Richards, F. M. *J. Biol. Chem.* **1983**, *258*, 3039.
(17) Patel, D. J.; Woodward, C. K.; Bovey, F. A. *Proc. Natl. Acad. Sci. U.S.A.* **1972**, *69*, 599.
(18) Konishi, Y.; Scheraga, H. A. *Biochemistry* **1980**, *19*, 1316.
(19) Baker, W. R.; Kintanar, A. *Arch. Biochem. Biophys.* **1996**, *327*, 189.
(20) Markley, J. L. *Biochemistry* **1975**, *14*, 3546.
(21) Markley, J. L. *Biochemistry* **1975**, *14*, 3554.
(22) Markley, J. L. *Acc. Chem. Res.* **1975**, *8*, 70.
(23) Markley, J. L.; Finkenstadt, W. R. *Biochemistry* **1975**, *14*, 3562.
(24) Santoro, J.; Juretschke, H. P.; Ruterjans, H. *Biochim. Biophys. Acta* **1979**, *578*, 346.
(25) Cole, R.; Loria, J. P. *Biochemistry* **2002**, *41*, 6072.
(26) Doucet, N.; Watt, E. D.; Loria, J. P. *Biochemistry* **2009**, *48*, 7160.
(27) Kovrigin, E. L.; Loria, J. P. *J. Am. Chem. Soc.* **2006**, *128*, 7724.
(28) Kovrigin, E. L.; Loria, J. P. *Biochemistry* **2006**, *45*, 2636.
(29) Watt, E. D.; Shimada, H.; Kovrigin, E. L.; Loria, J. P. *Proc. Natl. Acad. Sci. U.S.A.* **2007**, *104*, 11981.
(30) Hornak, V.; Abel, R.; Okur, A.; Strockbine, B.; Roitberg, A.; Simmerling, C. *Proteins: Struct., Funct., Bioinf.* **2006**, *65*, 712.
(31) Kabsch, W.; Sander, C. *Biopolymers* **1983**, *22*, 2577.
(32) Liu, Y. S.; Hart, P. J.; Schlunegger, M. P.; Eisenberg, D. *Proc. Natl. Acad. Sci. U.S.A.* **1998**, *95*, 3437.
(33) Picone, D.; Di Fiore, A.; Ercole, C.; Franzese, M.; Sica, F.; Tomaselli, S.; Mazzarella, L. *J. Biol. Chem.* **2005**, *280*, 13771.
(34) Fritz, D.; Koschke, K.; Harmandaris, V. A.; van der Vegt, N. F. A.; Kremer, K. *Phys. Chem. Chem. Phys.* **2011**, *13*, 10412.
(35) Ho, B. K.; Agard, D. A. *PLoS Comput. Biol.* **2009**, *5*, e1000343.
(36) Chandler, D. *Nature* **2005**, *437*, 640.
(37) Benkovic, S. J.; Hammes-Schiffer, S. *Science* **2003**, *301*, 1196.
(38) Davulcu, O.; Flynn, P. F.; Chapman, M. S.; Skalicky, J. J. *Structure* **2009**, *17*, 1356.
(39) Dutton, P. L.; Munro, A. W.; Scrutton, N. S.; Sutcliffe, M. J. *Philos. Trans. R. Soc. B* **2006**, *361*, 1293.
(40) Lipchock, J.; Loria, J. P. *J. Biomol. NMR* **2009**, *45*, 73.
(41) Onuchic, J. N.; Kobayashi, C.; Miyashita, O.; Jennings, P.; Baldridge, K. K. *Philos. Trans. R. Soc. B* **2006**, *361*, 1439.
(42) Pisliakov, A. V.; Cao, J.; Kamerlin, S. C. L.; Warshel, A. *Proc. Natl. Acad. Sci. U.S.A.* **2009**, *106*, 17359.
(43) Roca, M.; Messer, B.; Hilvert, D.; Warshel, A. *Proc. Natl. Acad. Sci. U.S.A.* **2008**, *105*, 13877.
(44) Mittermaier, A.; Kay, L. E. *Science* **2006**, *312*, 224.
(45) Eisenmesser, E. Z.; Millet, O.; Labeikovsky, W.; Korzhnev, D. M.; Wolf-Watz, M.; Bosco, D. A.; Skalicky, J. J.; Kay, L. E.; Kern, D. *Nature* **2005**, *438*, 117.
(46) Henzler-Wildman, K.; Kern, D. *Nature* **2007**, *450*, 964.
(47) Zegers, I.; Maes, D.; Daothi, M. H.; Poortmans, F.; Palmer, R.; Wyns, L. *Protein Sci.* **1994**, *3*, 2322.
(48) Baldwin, R. L. *J. Biol. Chem.* **2003**, *278*, 17581.
(49) Brown, J. E.; Klee, W. A. *Biochemistry* **1971**, *10*, 470.
(50) Ishima, R.; Torchia, D. A. *Nat. Struct. Mol. Biol.* **2000**, *7*, 740.
(51) Moon, S.; Case, D. *J. Biomol. NMR* **2007**, *38*, 139.
(52) Cuendet, M.; Michielin, O. *Biophys. J.* **2008**, *95*, 3575.
(53) Israelewitz, B. *Curr. Opin. Struct. Biol.* **2001**, *11*, 224.
(54) Israelewitz, B.; Baudry, J.; Gullingsrud, J.; Kosztin, D.; Schulten, K. *J. Mol. Graphics Modell.* **2001**, *19*, 13.
(55) Izrailev, S.; Stepaniants, S.; Balsera, M.; Oono, Y.; Schulten, K. *Biophys. J.* **1997**, *72*, 1568.
(56) Marszalek, P. E.; Lu, H.; Li, H.; Carrion-Vazquez, M.; Oberhauser, A. F.; Schulten, K.; Fernandez, J. M. *Nature* **1999**, *402*, 100.
(57) Sotomayor, M.; Schulten, K. *Science* **2007**, *316*, 1144.
(58) Lu, H.; Schulten, K. *Biophys. J.* **2000**, *79*, 51.
(59) Schulten, K. *J. Chem. Phys.* **1981**, *74*, 4426.
(60) Hsin, J.; Strümpfer, J.; Lee, E.; Schulten, K. *Annu. Rev. Biophys.* **2011**, *40*, 187.
(61) Case, D. A.; Cheatham, T. E.; Darden, T.; Gohlke, H.; Luo, R.; Merz, K. M.; Onufriev, A.; Simmerling, C.; Wang, B.; Woods, R. J. *J. Comput. Chem.* **2005**, *26*, 1668.
(62) http://boscoh.com/rip/.
(63) Frisch, M. J. et al. *Gaussian09*; Gaussian, Inc.: Wallingford, CT, 2009.
(64) Ditchfield, R. *Mol. Phys.* **1974**, *27*, 789.
(65) Cui, Q.; Karplus, M. *J. Phys. Chem. B* **2000**, *104*, 3721.